A Low-cost, Hand-held Stereoscopic Device for Measuring Dynamic Deformations of Skin In Vivo

Amir HajiRassouliha[1*], Barbara Kmiecik[2], Andrew J. Taberner[1,3], Martyn P. Nash[1,3], Poul M. F. Nielsen[1,3]
[1] Auckland Bioengineering Institute, [3] Department of Engineering Science, The University of Auckland, Auckland, New Zealand
[2] Department of Mechanics, Materials Science, and Engineering, Faculty of Mechanical Engineering, Wroclaw University of Technology, Wroclaw, Poland
[*] ahaj975@aucklanduni.ac.nz

Abstract: **Measuring the deformation of skin in vivo is useful in a number of applications. For example, the response of skin to a variety of mechanical loadings can provide information about the health of the underlying tissue. A number of devices have been developed for measuring the surface deformation of in vivo skin. However, existing devices are typically incapable of covering large areas of skin, or are expensive. To address these issues, we present the design and evaluation of a hand-held low-cost stereoscopic device for in vivo measurement of the dynamic surface deformation of skin. A camera rig with sufficient mechanical strength was designed to hold four high-speed synchronised cameras. The field of view (FOV) of the cameras is approximately 20 mm × 20 mm. A sample 2D deformation measurement of the surface of skin was performed to show the application of this device.**

Keywords: Stereoscopic device, in vivo skin, surface deformation measurement, hand-held device.

I. INTRODUCTION

Tracking the surface deformations of soft tissues (e.g. skin, and breast) can be used to help in investigations of tissue properties. The biomechanical properties of skin have been studied extensively for various applications [1][2], and computational modelling of skin was used to assist in studying wrinkling [3], simulating stretching and compression of skin for animations [4], simulating plastic surgery [5], and in the design of high-performance clothing [6].

Pioneering studies that have characterised the mechanical properties of in vitro skin were published in the 1970s. In 1973, Lanir and Fung analysed the mechanical behaviour of rabbit skin during biaxial tension tests [7], and tracked markers in a single camera image [8]. Skin is anisotropic and heterogeneous [9], and typically exhibits different characteristics between the in vivo and in vitro states. If one is interested in the behaviour of living skin, it is necessary to identify and measure detailed localised surface deformations in vivo. Even though biaxial tests are a common way of studying the mechanical properties of skin, such experiments are difficult to perform on in vivo human skin [10]. A number of alternative techniques, such as tissue compression [11], suction [12], and indentation [13], have also been used to estimate the mechanical properties of skin. Measurement devices such a micro-robot [14], a motion capture system [15], a single camera system [16], and a polarised LED sphere with macro camera [4], have been developed to measure in vivo skin surface deformations. However, motion capture systems (such as [15]) are unable to provide accurate measurements, single camera systems [4][16] can only cover flat, limited areas of skin, whereas the proposed micro-robot system [14] is complicated and expensive to build, and only can be used for small areas of skin. A comprehensive analysis of stretching and compression of large regions of skin would be possible if the dynamic deformations could be simultaneously captured from different viewing angles. To address this, we designed a low-cost, hand-held stereoscopic device to track in vivo dynamic deformations of skin using four different viewing angles. This portable device can be easily held in one hand to measure localised surface deformations over various parts of the body, such as the hand or face. Design considerations included the provision of a suitable field of view (FOV) for in vivo measurement of skin deformations, adequate depth of field (DOF) for good quality images, sufficient mechanical strength for the camera rig, and symmetric views for overlapping FOVs. We evaluated our device by capturing synchronised images of a hand from four different angles at 150 frames per second (fps), and estimating 2D deformations of the skin on the hand from sequential images.

II. CAMERA AND LENS SELECTION

The first step in designing a stereoscopic system is to select a suitable camera. Machine vision cameras are commonly used for measurement purposes. In general, the selection of a camera involves a trade-off between cost and other specifications, such as image resolution, maximum frame-rate, physical size, and the image quality. High-frame-rate cameras have the capability to record intermediate states of the skin during deformation. Therefore, they are preferable for in vivo measurement, where skin can often undergo complex and rapid deformations. Nonetheless, high-frame-rate cameras are typically expensive, and thus unsuitable for low-cost systems. For our stereoscopic device, we aimed for a reasonable trade-off between frame-rate and cost. The frame-rate (i.e. data throughput) and cost are primarily determined by the bus interface from the camera to the computer. Various camera bus interfaces are introduced in the following section, and used to determine a suitable selection for our application.

A. Selecting the camera bus interface

The main camera bus interfaces for PC-based systems include [17]:

- FireWire (IEEE 1394);
- Gigabit Ethernet (GigE);

978-1-5090-0357-0/15/$31.00 ©2015 IEEE

- Camera Link;
- Universal Serial Bus (USB 2 and USB 3).

FireWire is a serial bus interface for high-speed communications (FireWire is the name chosen by Apple Inc. for IEEE 1394 interface standard). The IEEE 1394a provides 40 MB/s data transfer rate [17], which is not sufficient for high frame-rate applications. Since the establishment of the USB interface as the standard port in PCs, the FireWire interface is no longer generally available in PCs. Therefore, FireWire cameras are not a suitable choice for our system. Even though Apple Inc. introduced Thunderbolt [18] in 2011 to replace FireWire, machine vision cameras that incorporate the Thunderbolt interface have only been introduced very recently [19], and are not yet available in the market.

GigE uses a standard Ethernet port for data communication. The maximum theoretical bandwidth of GigE is 125 MB/s [17], which is insufficient for frame-rates higher than 100 fps for a reasonable camera image size, hence unsuitable for our system.

The Camera Link interface was the first standard developed for high-speed data transfer for digital cameras in industrial applications. The Camera Link interface has three bandwidth configurations designed for different applications i.e. the base, medium, and full bandwidth configurations. The data transfer rate for these Camera Link configurations are summarised in Table I.

TABLE I. CAMERA LINK BANDWIDTH CONFIGURATIONS

Configuration	Data rate (Gbit/s)	Data rate (MB/s)
Base	2.04	255
Medium	4.08	510
Full	5.44	680

Although the Camera Link base configuration specifies a relatively high data transfer rate (i.e. 255 MB/s), the majority of cameras achieve only about 100 MB/s, which is not suitable for frame-rates higher than 100 fps. However, the Camera Link medium and full bandwidth configurations provide a sufficient data transfer rate for high frame-rate applications. Some of the advantages of the Camera Link interface are:

- transmission of image data is independent of the CPU and the operating system; hence cameras can be hardware triggered without any latency;
- synchronisation between Camera Link cameras is straightforward;
- the camera settings can be controlled using Camera Link drivers;
- frame grabbers manage image data transmission to local memory via direct memory access (DMA), which does not overload the CPU;
- frame grabbers have processing units that are able to perform basic processing on the image data at high-speed.

Limitations of the Camera Link interface include:

- Camera Link is not a standard PC interface, hence frame grabber cards are needed for transferring the image data from the camera to the host PC;
- Camera Link cameras, frame grabbers, cables and accessories are typically expensive;
- New hardware technologies rapidly outdate camera Link frame grabbers.

Even though the medium and full configurations of the Camera Link interface may be suitable options for our stereoscopic system, we did not choose these options as the camera bus interface of our device due to the above limitations.

The USB 3 vision standard (also known as SuperSpeed USB) was published in January 2013 for use in camera systems. USB 3 vision has a number of improvements over USB 2, such as the cable locking option, higher bandwidth, lower CPU demand, increased power delivery, and reduced power consumption [20]. The theoretical data transfer rate using USB 3 vision is 5 Gb/s (i.e. 625 MB/s). The USB 3 vision interface is rapidly growing in popularity, and has become the primary choice for cost-effective solutions. Some of the advantages of the USB 3 interface are that:

- the USB 3 interface is now a standard port, hence frame grabber cards are not needed for USB 3 cameras;
- USB 3 cameras, cables and accessories are typically low-cost;
- the USB 3 interface can provide power over the data cable, which eliminates the need for a separate power source;
- USB 3 cameras can transfer image data directly to the host memory via DMA with no overload on the CPU.

Nevertheless, USB 3 also has limitations:

- although the theoretical data transfer rate using USB 3 is 625 MB/s, it is in practice limited to 400 MB/s;
- USB 3 vision does not support frame grabbers; thus synchronisation of USB 3 cameras is more challenging in comparison to Camera Link cameras.

Table II shows a comparison between the key technical features of the Camera Link and USB 3 vision interfaces. Even though the data transfer rate of USB 3 is less than the Camera Link interfaces, the difference is not critical for measuring dynamic surface deformations. In addition, the maximum cable length of USB 3 is sufficient for PC-based applications. Therefore, considering the lower price of USB 3 cameras and accessories in comparison to the Camera Link interface, we chose USB 3 as the camera interface of our stereoscopic device.

TABLE II. KEY FEATURES OF CAMERA LINK AND USB3

Camera interface	Data transfer rate (MB/s)	Maximum cable length (m)
Camera Link	510 or 680	10
USB 3	400	5

B. *Selecting the camera and lens*

Monochrome USB 3 cameras from Point Grey (FL3-U3-13Y3M-C) were selected for our device [21]. The maximum frame-rate of these cameras is 150 fps, and the maximum image resolution is 1280 pixel × 1024 pixel. Therefore, the maximum data transfer of these cameras is 196.6 MB/s, which is approximately half of the maximum bandwidth of the USB 3 vision interface (Table II). The single unit price of FL3-U3-13Y3M-C cameras is USD $595 [22]. In comparison, the single unit price for a Camera Link camera with 150 fps from Point Grey (GZL-CL-41C6M-C) is USD $2195 [23]; moreover, a frame grabber card, which typically costs around USD $700 [24], is also needed for a Camera Link camera.

The next step is to select the camera lens. Short focal length lenses provide a large angle of view (AOV) for the cameras (i.e. a large FOV at a constant distance to the camera); thus such lenses can allow the physical dimension of the camera setup to be more compact for a particular FOV. Nevertheless, short focal length lenses usually have a high level of barrel distortion, which may cause inaccuracies in deformation measurements. To strike a balance between having a reasonable physical dimension for the camera setup, and an acceptable range of barrel distortion, 6 mm focal length lenses were chosen for our stereoscopic system (DF6HA-1B from Fujifilm). This lens provides 44.54° AOV for FL3-U3-13Y3M-C cameras.

III. Camera Rig Design

The mechanical design of our hand-held stereoscopic device considered the following criteria:

- The FOV should be approximately 200 mm × 200 mm to cover an adequate surface area of the skin from different viewing angles;
- The cameras should have large enough overlapping FOVs for measuring skin deformations in 3D. Each part of the skin must be imaged with at least two cameras to reconstruct the deformations in 3D;
- The angle between different camera axes at the centre of the FOV should be close to 90°. Orienting the cameras in this way results in isotropic pixel resolution;
- The physical dimensions and mass of the stereoscopic system should be small enough to be portable and hand-held;
- The rig should have enough mechanical strength to hold the cameras rigidly during hand-held use;
- The rig should be constructed using cost-effective materials and processes.

A ring arrangement for the cameras is a suitable configuration for tracking the skin deformations from different viewing angles. We chose to use four cameras arranged as two opposite pairs to cover the object. Increasing the number of cameras would improve the 3D reconstruction process, but it would also make the device more expensive and heavier. Based on the mentioned design specifications, the positions of the four cameras were calculated, and a camera rig was developed.

A. *Determining the cameras positions*

The focal length of the camera lens is equivalent to the distance between the back principal point of the lens and the camera image plane. Therefore, the back principal point is the physical location of the focal point of the camera. The positions of the two cameras in one opposite pair were calculated by considering the target FOV of 200 mm × 200 mm, the required 90° angle between the axes of the cameras at the centre of the FOV, and the AOV of the lens (Fig. 1). In the design in Fig. 1, the distance between the opposing cameras is 276 mm, and the height of the principal points is 138 mm. The same design was used for the other pair of cameras. Note that the FOV is trapezoidal for a rectangular camera image plane (Fig. 2).

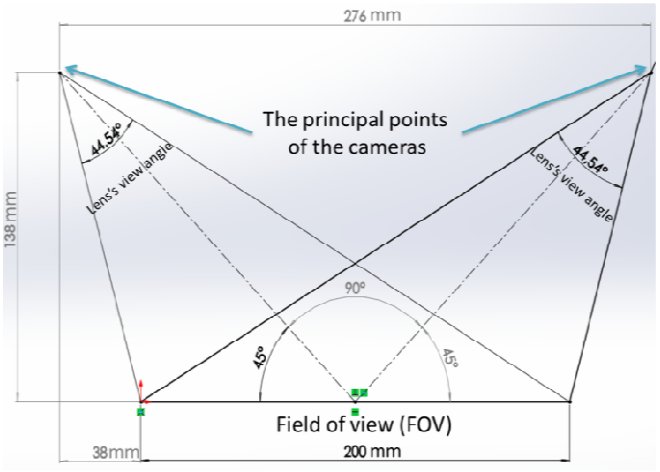

Fig. 1. The positions of the focal points of an opposing pair of FL3-U3-13Y3M-C cameras. This arrangement provided a 200 mm field of view with a 6 mm lens (angle of view of 44.54°). The axes of the cameras intersect at an angle of 90° at the centre of the field of view.

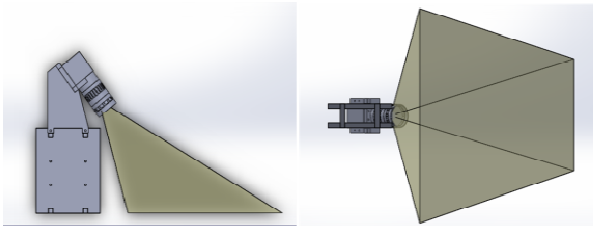

Fig. 2. Schematic representation of the trapezoidal shape of the camera field of view for a rectangular camera image plane.

B. *Design of the camera rig*

The rig needed to accommodate the four cameras in the positions calculated in Section III.A. The geometric specification of the camera rig should satisfy the conditions discussed in section III. After several iterations, the design illustrated in Fig. 3 was selected for our device. In this design, all of the components were separate 2D parts, which were assembled to build the 3D rig. As Fig. 3 illustrates, the cameras were arranged in in a ring configuration with two pairs of opposing cameras. Four LEDs were used to illuminate the surface of the skin. The LEDs were positioned on a circular rail, enabling the height and position of LEDs to be adjusted to

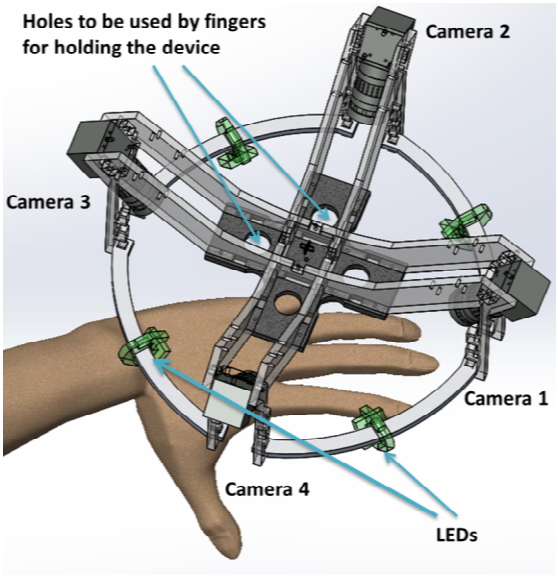

Fig. 3. The design of our stereoscopic device. Four cameras were placed in a ring configuration in two opposite pairs. The heights and the distances between the cameras were chosen based on the calculations in Section III.A.

manage the direction of the light for objects of differing shapes. Each camera was connected to the central plate of the device using two curved plates to ensure sufficient mechanical strength. The curved plates were attached and fixed to the central plate in an inter-locking manner as shown in Fig. 4. The connections were glued to ensure that the camera rig was sufficiently stable. It is also possible to screw the curved plates to the central plate (Fig. 4). The cameras were fixed to the curved plates with attachments and screws as shown in Fig. 5.

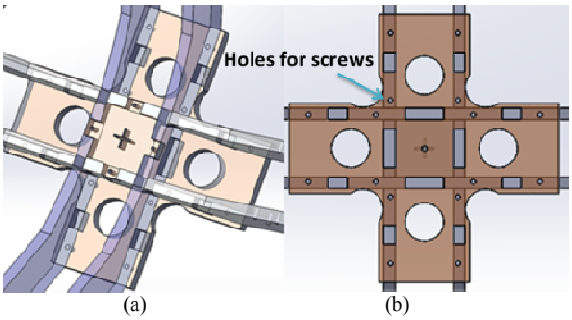

(a) (b)

Fig. 4. The top view (a) and the bottom view (b) of the central plate of the design. The curved plates were fixed and glued to this central plate in an inter-locking manner. It is also possible to screw the curved plates to the central plate.

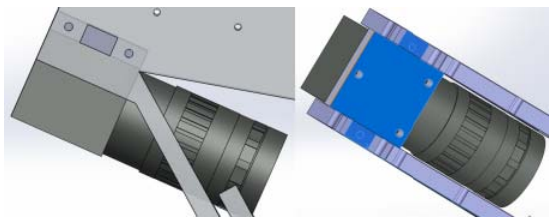

(a) (b)

Fig. 5. The side view (a) and bottom view (b) of the camera attachments to the curved plates.

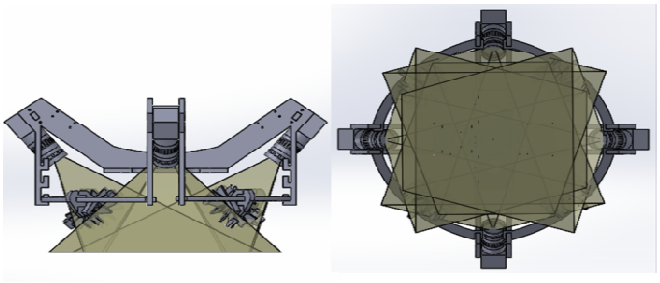

(a) (b)

Fig. 6. The side view (a) and bottom view (b) of the fields of view of each of the four cameras. The overlapping FOV of the cameras can be seen in the central part of panel (b).

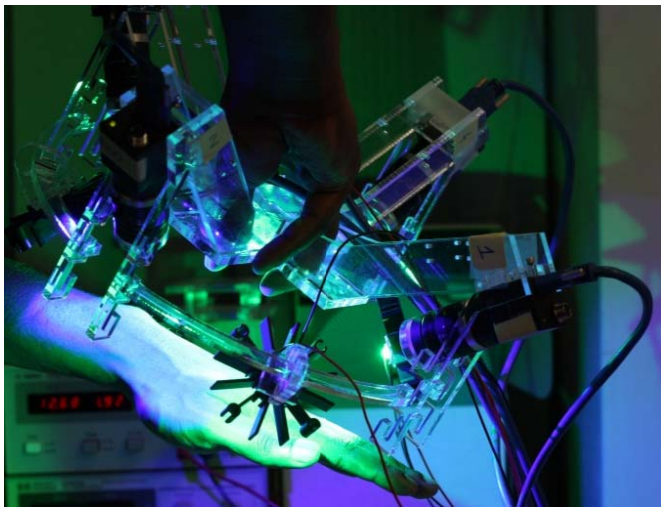

Fig. 7. Our hand-held stereoscopic device for in vivo measurement of skin surface deformations.

The camera FOV is trapezoidal in shape. Figure 6 shows the FOV for each of the four cameras of our stereoscopic device. The overlapping FOV can be seen in the central part in Fig. 6(b).

After finalising the design, a laser cutter was used to cut sheets of acrylic glass (plexiglass) to build the 2D components of our camera rig. The acrylic sheets were 6 mm thick to provide a reasonable trade-off between mechanical strength and weight for the camera rig. Figure 7 shows the final hand-held stereoscopic device.

To compare the theoretical calculation of the FOV with the measured FOV, tests were carried out with our hand-held stereoscopic device, and the results confirmed the validity of our theoretical calculations for each camera.

C. Mass

The mass of the portable part of our stereoscopic device was approximately 2 kg. By including the approximate mass of four cameras (each 52 g), four lenses (each 55 g), USB 3 cables (each 150 g), and LED heat sinks (each 60 g), the total mass of the portable device was approximately 3 kg.

IV. Camera Settings

A. Depth of field (DOF)

DOF is the distance between the nearest and farthest objects that have a sharp focus (i.e. are not blurred). Equation 1 shows how the DOF of a lens can be approximated [17]:

$$\text{DOF} \cong \frac{2 \times C \times F_n \times f_d \times (f_d - f)}{f^2} \quad (1)$$

where C is the acceptable diameter of the circle of confusion (i.e. the smallest part of the image which is acceptably sharp), F_n is the F-number of the lens (i.e. the ratio of the focal length to the diameter of the pupil of the lens), f_d is the distance for which the lens is focused, and f is the focal length of the lens. For predefined FOV dimensions with a fixed focal length lens (such as DF6HA-1B), the F-number is the main factor that determines the DOF. Larger F-numbers result in sharper camera images. However, since the pupil size is smaller for larger F-numbers, more light is needed to illuminate the object. Based on the design of our stereoscopic device, the maximum DOF in the overlapping FOV was less than 240 mm. The focusing distances of the lenses were set at the centre of the overlapping FOV (174 mm from the lenses), and the permissible circle of confusion for our cameras was 15 µm based on the camera data sheet. Substituting these values into Equation 1, provided the acceptable F-number for the cameras in our stereoscopic device as $F_n = 9.85$. Therefore, we chose the F-number to be 10 for the lenses of our cameras.

B. Illumination

Cameras needed adequate light for the F-number of 10 at 150 fps. The camera specification in the datasheet shows that the camera sensor has a high sensitivity to the wavelengths close to the green colour. Thus, four super-bright (750 lm) green LEDs were chosen for our hand-held device. The LEDs could be changed to other colours depending on the optical characteristics of the tissue. Circular polarising filters were used for each camera to reduce specular reflections, which may be caused by super-bright LEDs.

C. Capturing image data and synchronising the cameras

Equation 2 and Equation 3 show the required data transfer rates when using one and four USB 3 cameras (FL3-U3-13Y3M-C) at 150 fps, respectively.

$$\text{Data transfer rate (one camera)} = \frac{150\ fps \times 1280\ pixel \times 1024\ pixel \times 8\ bit}{8} \cong 196.6\ MB/s \quad (2)$$

$$\text{Data transfer rate (four cameras)} = 196.6\ MB/s \times 4 = 786.4\ MB/s \quad (3)$$

Our tests showed that the storage rates for a SATA hard drive and for a solid-state drive (SSD) were approximately 42.5 MB/s, and 177.5 MB/s, respectively. Therefore, these hard drive technologies were not suitable for storage of the image data from the four cameras. Instead, the image data were first buffered in DDR3 RAM of the PC during recordings, and subsequently transferred to the hard drive. The storage rate of DDR3 RAM is approximately 1 GB/s, which is adequate to simultaneously capture the image data from all four cameras. This approach obviously limits the recording time to the amount of available DDR3 RAM. For instance, the recording time for a PC with 32 GB DDR3 RAM is limited to less than 40 seconds. If longer recording times were required, it would be possible using double buffering between DDR3 RAM and the hard drive. In this study, the 40 seconds recording duration is sufficient for measuring dynamical skin deformations at high frame-rates.

The cameras were simultaneously triggered in software via separate CPU threads to capture synchronised data. A digital millisecond timer was used to verify the synchronisation of the cameras for the duration of our recordings (the maximum recording duration was 30 seconds for these tests).

V. In Vivo Surface Deformation Measurement

Figure 8 shows an example of the images of a hand from each of the four cameras in our hand-held stereoscopic device. As shown in Fig. 8, the cameras were able to span the entire hand from different viewing angles. This demonstrated that the illumination and the *F-number* of the cameras were appropriately selected to provide good quality images with sufficient sharpness.

Figure 9 shows an example of measuring 2D displacement of the skin on the hand for two sequential images captured at 150 fps. The displacements were measured using the sub-pixel image registration algorithm developed by our group (unpublished). The displacements were measured by tracking the intrinsic features of the skin (i.e. application of an artificial texture was not required). The displacement vectors are superimposed on the image, and the magnitudes of the displacement values were indicated using a colour spectrum.

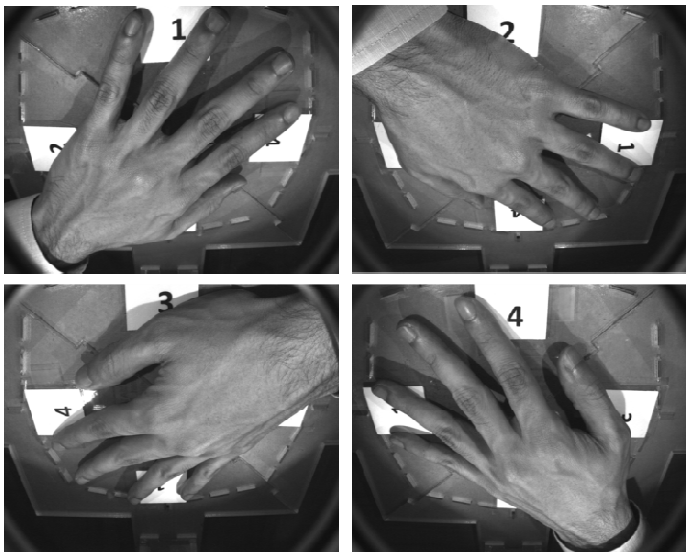

Fig. 8. Images of a hand from each of the four cameras of our hand-held stereoscopic device. The camera images spanned the whole surface of the hand from each of the four viewing angles.

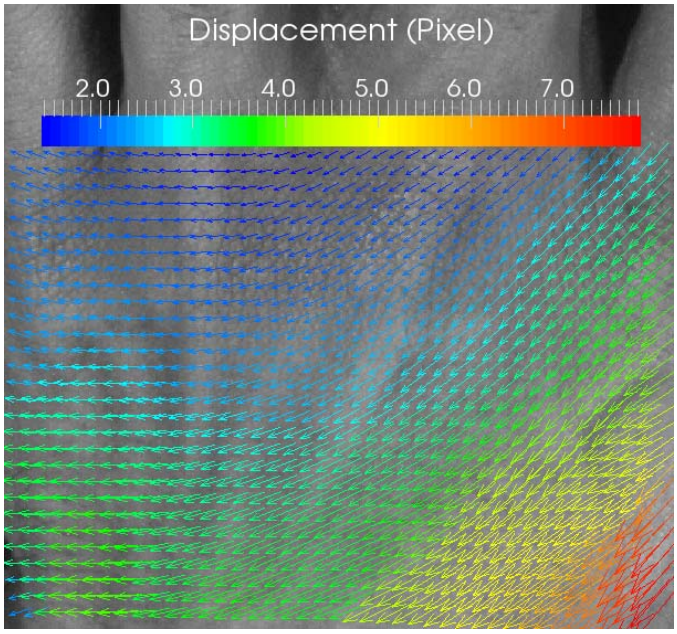

Fig. 9. A sample 2D displacement measurement from the surface of the skin using two sequential images of the hand for one of the cameras of our device.

VI. Conclusions and Future Works

This paper describes the design of a hand-held stereoscopic device for measuring in vivo skin deformation from different viewing angles. The results showed that the cameras can capture synchronised images from a FOV of approximately 20 mm × 20 mm. The camera and lighting parameters were chosen appropriately to provide good quality images. The total mass of our device was approximately 3 kg, and the hardware cost was less than USD $3000 for four cameras and their lenses. Thus, our device is a suitable cost-effective hand-held setup for measuring skin deformation of various parts of the body. Even though the displacement measurements were performed in 2D (Fig. 9), the cameras of our device have sufficient overlapping FOV (Fig. 6) to enable us to extend the measurements to 3D. We intend to perform 3D measurements of skin surface deformations using our device in future studies.

References

[1] J. W. Y. Jor, M. D. Parker, A. J. Taberner, M. P. Nash, and P. M. F. Nielsen, "Computational and experimental characterization of skin mechanics: identifying current challenges and future directions.," *Wiley Interdiscip. Rev. Syst. Biol. Med.*, vol. 5, no. 5, pp. 539–56, 2013.

[2] C. Flynn, A. Taberner, and P. Nielsen, "Modeling the mechanical response of in vivo human skin under a rich set of deformations," *Ann. Biomed. Eng.*, vol. 39, no. 7, pp. 1935–1946, 2011.

[3] C. Flynn and B. A. O. McCormack, "Simulating the wrinkling and aging of skin with a multi-layer finite element model," *J. Biomech.*, vol. 43, no. 3, pp. 442–448, 2010.

[4] K. Nagano, G. Fyffe, O. Alexander, J. Barbič, L. Abhijeet, and G. Paul, "Skin Microstructure Deformation with Displacement Map Convolution," *ACM Trans. Graph. Vol. 34, No. 4, Artic. 109*, pp. 1–10, 2015.

[5] M. Pawlaczyk, M. Lelonkiewicz, and M. Wieczorowski, "Age-dependent biomechanical properties of the skin.," *Post□py dermatologii i Alergol.*, vol. 30, no. 5, pp. 302–6, Oct. 2013.

[6] H. Lee, K. Hong, and Y. Lee, "Ergonomic mapping of skin deformation in dynamic postures to provide fundamental data for functional design lines of outdoor pants," *Fibers Polym.*, vol. 14, no. 12, pp. 2197–2201, Jan. 2014.

[7] Y. Lanir and Y. C. Fung, "Two-dimensional mechanical properties of rabbit skin—I. Experimental system," *J. Biomech.*, vol. 7, no. 1, pp. 29–34, 1974.

[8] Y. Lanir and Y. C. Fung, "Two-dimensional mechanical properties of rabbit skin—II. Experimental results," *J. Biomech.*, vol. 7, no. 2, pp. 171–182, 1974.

[9] A. Ní Annaidh, K. Bruyère, M. Destrade, M. D. Gilchrist, and M. Otténio, "Characterization of the anisotropic mechanical properties of excised human skin.," *J. Mech. Behav. Biomed. Mater.*, vol. 5, no. 1, pp. 139–48, Jan. 2012.

[10] Y. A. Kvistedal and P. M. F. Nielsen, "Estimating material parameters of human skin in vivo," *Biomech. Model. Mechanobiol.*, vol. 8, no. 1, pp. 1–8, 2009.

[11] J. Li, H. Liu, K. Althoefer, and L. D. Seneviratne, "A stiffness probe based on force and vision sensing for soft tissue diagnosis," *Proc. Annu. Int. Conf. IEEE Eng. Med. Biol. Soc. EMBS*, vol. 1, pp. 944–947, 2012.

[12] S. Diridollou, F. Patat, F. Gens, L. Vaillant, D. Black, J. M. Lagarde, Y. Gall, and M. Berson, "In vivo model of the mechanical properties of the human skin under suction.," *Skin Res. Technol.*, vol. 6, no. 4, pp. 214–221, 2000.

[13] C. Pailler-Mattei, S. Bec, and H. Zahouani, "In vivo measurements of the elastic mechanical properties of human skin by indentation tests.," *Med. Eng. Phys.*, vol. 30, no. 5, pp. 599–606, Jun. 2008.

[14] C. Flynn, A. J. Taberner, P. M. F. Nielsen, and S. Fels, "Simulating the three-dimensional deformation of in vivo facial skin.," *J. Mech. Behav. Biomed. Mater.*, vol. 28, pp. 484–94, Dec. 2013.

[15] J. Mahmud, S. L. Evans, and C. A. Holt, "An Innovative Tool to Measure Human Skin Strain Distribution in Vivo using Motion Capture and Delaunay Mesh," *J. Mech.*, vol. 28, no. 02, pp. 309–317, May 2012.

[16] S. Kacenjar, S. Chen, M. Jafri, B. Wall, R. Pedersen, and R. Bezozo, "Near real-time skin deformation mapping," *SPIE-IS&T*, vol. 8655, Feb. 2013.

[17] C. Demant, B. Streicher-Abel, and C. Garnica, *Industrial Image Processing*. Berlin, Heidelberg: Springer Berlin Heidelberg, 2013.

[18] https://thunderbolttechnology.net/

[19] http://www.ximea.com/en/products-news/thunderbolt-camera-imx174-cmv20000

[20] http://ww2.ptgrey.com/_PGR_Uploads/PGRNA/files/USB3_Improvements_over_USB2_v2.pdf

[21] http://www.ptgrey.com/flea3-13-mp-mono-usb3-vision-vita-1300-camera

[22] http://www.ptgrey.com/flea3-usb3-vision-cameras

[23] http://www.ptgrey.com/gazelle-camera-link

[24] http://www.epixinc.com/products/pixci_eb1mini.htm